Interpretation of the magnetic susceptibility behaviour of soft carbon steels based on the scaling theory of second order phase transitions for systems with supercritical disorder

A. Skarlatos, A. Martínez-De-Guerenu, D.J. Badiola, I. Lelidis

Interpretation of the magnetic susceptibility behaviour of soft carbon steels based on the scaling theory of second order phase transitions for systems with supercritical disorder

A. Skarlatos[a], A. Martínez-de-Guerenu[b,c], D. J. Badiola[b,c], I. Lelidis[d]

[a] *Université Paris-Saclay, CEA, List, F-91120, Palaiseau, France*
[b] *CEIT-Basque Research and Technology Alliance (BRTA), Manuel de Lardizábal 15, 20018 Donostia / San Sebastián, Spain*
[c] *Universidad de Navarra, Tecnun, Manuel de Lardizábal 13, 20018 Donostia / San Sebastián, Spain*
[d] *National and Kapodestrian University of Athens, Physics Department, Panepistimiopolis, Zografou, 15784 Athens, Greece*

Abstract

The experimental magnetic susceptibility curves of several soft steel grades, like interstitial free (IF) or low carbon (LC) steels, can be interpreted within the framework of universal scaling functions obtained for systems with quenched disorder, such as the one described by the random field Ising model with supercritical disorder. Mean-field theory (both scalar and site-dependent) is used to explore the behaviour at the proximity of the coercive field, and explicit expressions are derived. As a result, the susceptibility values close to the coercive field can be approximated to a good extend by a Lorentzian function. Theoretical results are compared against a number of experimental curves obtained from interstitial free (IF) and extra low carbon (ELC) steels subjected to isothermal annealing.

Keywords: random field Ising model, Lorentz function, magnetic susceptibility, isothermal annealing, recovery process

1. Introduction

Differential magnetic susceptibility measurements for soft industrial steel grades, like interstitial free (IF) and low or extra-low carbon (LC, ELC) steels, obtained during recovery, reveal a number of common features, among them, a notable resemblance of the susceptibility profile for external magnetic field values close to the coercive field [1–3].

The evolution of several magnetic indicators with the annealing temperature and holding time indicated in the above cited articles reveals the underlying link between the steel microstructure and the magnetic properties, which makes them a good tool for the monitoring of the recovery process. It is thus tempting to try to establish the aforementioned relation between structure and magnetic properties on a more solid theoretical background.

The recovery process during the isothermal annealing of steels is characterised by more-or-less constant grain sizes, with the effect of the heating acting primarily in enhancing the mobility of the dislocations yielding an overall softening of the material. One has thus to deal with a reasonably well-controlled microstructure whose main tuning variable is the dislocation density. These are quite favourable conditions, which satisfy to a good extend the main assumptions of the random-field Ising model (RFIM) making the latter a good candidate for the theoretical study of the problem, despite its simplicity [4–6].

A considerable amount of work has been published on that model, and a good understanding has been established thanks to the pioneering work of Sethna, Dahmen, Perkovic et al. [7–10]. In these articles it is shown that the random field (characterised by a disorder parameter R) plays the role of a tuning parameter in a second order phase transition. As a consequence, a critical disorder value R_c exists, around which the magnetization curve can be described by a scaling law of the following form

$$M - M[H_c(R_c)] \sim r^{\beta} \mathscr{M}_{\pm}\left(h/r^{\beta\delta}\right) \tag{1}$$

where H_c is the coercive field value at the critical disorder, r and h the normalised distance of the disorder and the magnetic field from their respective critical values, and $\mathscr{M}_{\pm}$ stands for a universal scaling function with β, δ giving the corresponding critical exponents at the transition. The $\pm$ sign in the index denotes the side across the critical point that is considered.

Following this line of reasoning, the susceptibility profile around H_c can be interpreted in terms of the scaling function $\mathscr{M}_{\pm}$, whose explicit form we try to derive in this article from the mean-field RFIM theory and confirm via comparison with numerical data obtained by a site-dependent mean-field model. The explicit relation between disorder and the maximum susceptibility value is also established by resorting to both analytical and numerical results using the site-dependent mean-field (SDMF) approach.

Given this link between susceptibility and disorder, one can address at a second level the experimentally established relation between susceptibility and annealing condi-

tions in order to indirectly relate the microstructural evolution (characterised by the material disorder) with the annealing conditions. This idea is explored in the second part of the article, where the experimental results of Martinez-de-Guerenu et al. are used to confirm on one hand the Lorentzian susceptibility profile, and to examine common trends between the annealing temperature and holding time with the disorder.

2. Theory

2.1. Mean-field theory

We consider an Ising spin system submerged to a constant random field. Such a system is described by the following Hamiltonian [7–9]

$$\mathcal{H} = -\frac{1}{2}J\sum_{\{i,j\}}\sigma_i\sigma_j - g\mu_B\sum_i(H+H_i)\sigma_i \tag{2}$$

where σ_i is the spin at the ith site of the Ising lattice, J stands for the exchange constant (which is considered invariant throughout the system lattice), μ_B is the Bohr's magneton, g is the gyromagnetic ratio, H is the applied (external) field, and H_i stands for the random field at the ith lattice site. Note that the $\{i,j\}$ index implies summation over the first neighbours.

Following the literature, we shall assume that the random field is described by a Gaussian distribution, acknowledging, however, that other distributions can be applied as well (yet with a minor impact to the results) [7]

$$\rho(H_i) = \frac{1}{\sqrt{2\pi}R}e^{-H_i^2/2R^2}. \tag{3}$$

R in (3) stands for the distribution variance, which is also a measure of the field randomness, or equivalently the degree of the system disorder.

Applying the mean-field theory approximation, the exact Hamiltonian (2) reduces to

$$\mathcal{H} = -\sum_i\left[Jzm + g\mu_B(H+H_i)\right]\sigma_i \tag{4}$$

with z being the coordination number, which for the 3D case is equal to 6, and m the mean spin (or normalised magnetisation)

$$m = <\sigma> = \frac{<M>}{M_s}. \tag{5}$$

M_s stands for the magnetisation at saturation. In order to simplify the notation, we proceed to the following normalisation for the magnetic field

$$h_i := g\mu_B H_i/J \tag{6}$$

and the same for H. Upon substitution in the Hamiltonian, we obtain the following simplified form

$$\mathcal{H}/J = -\sum_i\left(zm + h + h_i\right)\sigma_i \tag{7}$$

and the random field distribution becomes

$$\rho(h_i) = \frac{1}{\sqrt{2\pi}r}e^{-h_i^2/2r^2} \tag{8}$$

with the normalised disorder

$$r := g\mu_B R/J \tag{9}$$

In the rest of the article, lower-case letters, such as h, h_i and r will imply normalised variables. At zero-temperature, the mean-field approximation for the mean magnetisation m reads

$$m(h) = 1 - 2\int_{-\infty}^{-zm(h)-h}\rho(h_i)\,dh_i. \tag{10}$$

For disorder values lower than a critical value r_c (10) has a non-unique solution at $h = 0$, and the corresponding $m(h)$ presents a jump there. For $r > r_c$ the resulting curve is smooth and single valued at $h = 0$. This effect is illustrated in Fig. 1a , where the solution of (10) is drawn for different values of the disorder r. The magnetisation jump at $h = 0$ as a function of the normalised distance from the critical disorder $1 - r/r_c$ is also shown in Fig. 1b.

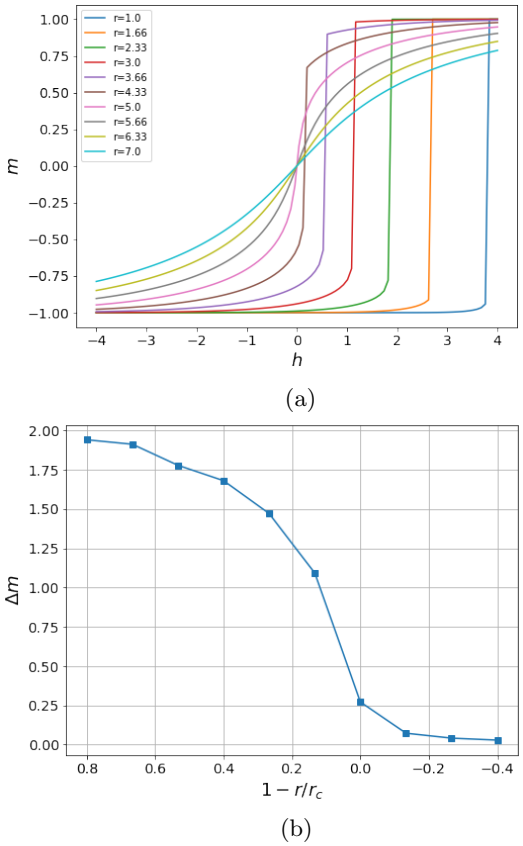

Figure 1: (a) Mean-field solution for the magnetisation curve for different disorder values. (b) Magnetisation jump at zero field as a function of the distance from the critical disorder $1 - r/r_c$. The critical disorder value can be estimated as $r_c \approx 5$.

This transition from a discontinuous to continuous variation presents all the characteristics of a second-order phase transition with the magnetisation jump δm at zero field playing the role of the order parameter. This transition has been exhaustively studied in the papers of Sethna, Dahmen et al. [7–9, 11, 12].

In the following analysis, we shall be interested in systems with supercritical disorder, i.e. we will consider the case where $r > r_c$. As explained above, for these disorder values the magnetisation curve is smooth around $h = 0$. Deriving (10) with respect to the external magnetic field h we obtain

$$\frac{dm}{dh} = 2\rho(zm + h)\left(z\frac{dm}{dh} + 1\right). \tag{11}$$

Setting $dm/dh = \chi$ and isolating the latter, we arrive at the following explicit expression for the susceptibility

$$\chi(h) = \frac{2\rho(zm + h)}{1 - 2z\rho(zm + h)} \tag{12}$$

or equivalently

$$\chi(h) = \frac{1}{[2\rho(zm + h)]^{-1} - z}. \tag{13}$$

Substituting the expression of the random field distribution from (3) yields

$$\chi(H) = \frac{1}{\sqrt{\frac{\pi}{2}} r\, e^{(zm+h)^2/2r^2} - z}. \tag{14}$$

Assuming that sum $zm + h$ admits small values with respect to the system disorder, we can develop the exponential function in Taylor series and keep only the first (linear) term, which will lead us to the approximation

$$\chi(H) \approx \frac{1}{\sqrt{\frac{\pi}{2}} r - z + \sqrt{\frac{\pi}{2}} \frac{1}{2r} (zm + h)^2}. \tag{15}$$

Since $(m, h) = (0, 0)$ is point of the solution described by the implicit expression (10), $m + h \approx 0$, implies that both h and m should be small. Let us thus write

$$m(h) \approx \chi_0 h \tag{16}$$

with χ_0 being the slope of the $m(h)$ curve at $h = 0$. Substitution of (16) upon (15) yields for small field values

$$\chi(h) \approx \frac{1}{\sqrt{\frac{\pi}{2}} r - z + \sqrt{\frac{\pi}{2}} \frac{1}{2r} (z\chi_0 + 1)^2 h^2}. \tag{17}$$

With slightly term rearrangement, (17) can be brought in the more compact form

$$\chi(h) \approx \frac{\chi_0}{1 + (h/\gamma)^2} \tag{18}$$

which is the Lorentzian distribution with χ_0 being the magnetic susceptibility at $h = 0$

$$\chi_0 = \left(\sqrt{\frac{\pi}{2}} r - z\right)^{-1} \tag{19}$$

and

$$\gamma = \left(\frac{2}{\pi}\right)^{1/4} \sqrt{\frac{2r}{\chi_0}} \frac{1}{(z\chi_0 + 1)}. \tag{20}$$

Having a closed form expression for the magnetic susceptibility, the corresponding expression for the magnetisation can be easily obtained by integration over h, which yields

$$m = \chi_0 \gamma \arctan\left(\frac{h}{\gamma}\right). \tag{21}$$

In order to test the accuracy of this approximation, the results obtained using the expression (18) are compared against the numerical solution of the implicit form (10) in Fig. 2. As one can see from the comparison, (18) yields a very satisfactory description of the susceptibility variation for small fields.

We observe that the derived approximation becomes more accurate at higher field values for increasing r. This conclusion is not surprising regarding the profile of the exact solution in Fig. 1a. In fact, the magnetisation around $h = 0$ becomes increasingly non-linear for smaller r values, which results in a varying slope in the domain of moderate fields. As a consequence, the approximation (16) does not hold for small disorder values just above the critical value except for the immediate neighbourhood of $h = 0$. The numerical results of (10) (exact solution) are compared in Fig. 2 with the Lorentzian function that is calculated using the asymptotic expression of (18) and the one obtained via least-square fit to the exact curve. It turns out that the two approaches yield more or less equivalent results for weak disorders, like the one in Fig. 2a. Note that for more significant r values, the best-fit curve provides a reasonable approximation of the exact numerical solution for the entire h-window, at the expense of a less accurate peak value. This fact signifies that the exact solution is closer to the Lorentzian form for a broader range of h values.

The mean-field approximation, used in the above analysis, does not support hysteresis since the implicit evaluation of (10) is a single-valued curve. To introduced hysteresis, (18) can be generalised by shifting the zero of the magnetisation curve to the coercive field (it is the point where m becomes small and hence the main arguments of the analysis hold), obtaining the expression

$$\chi(h) \approx \frac{\chi_c}{1 + [(h - h_c)/a]^2}. \tag{22}$$

where h_c stands for the coercive field and χ_c the corresponding susceptibility. In principle, (19) cannot be applied anymore in order to relate the susceptibility at the coercive field with the random field parameters. Their correlation, can, however, be established numerically by least-square fit, as done in (2).

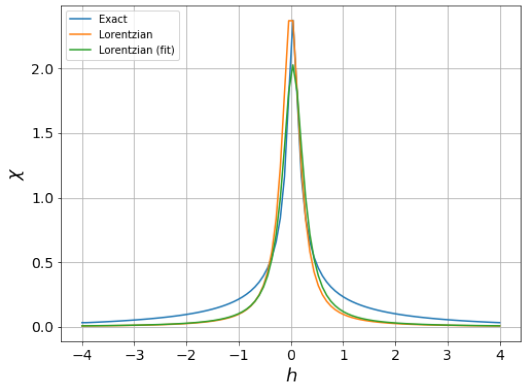

(a)

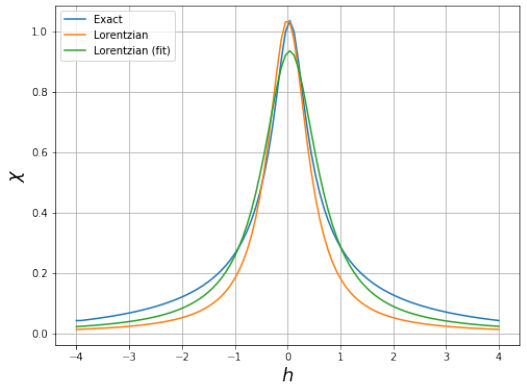

(b)

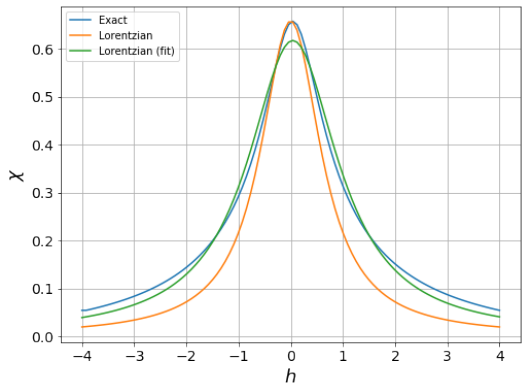

(c)

Figure 2: Comparison of the exact solution (10) ("Exact") with the expression (18) ("Lorentzian") and a fitted Lorentzian ("Lorentzian fit") for three different disorder values. (a) $r = 5.11$, (b) $r = 5.55$ and (c) $r = 6.0$.

Such generalisation of the mean-field results to hysteretic curves, is a heuristic approach. Nonetheless, some more rigorous justification can be sought by using the results of the site-dependent mean-field solution (SDMF), which natively introduced multi-branch solutions, and thereby hysteresis. This will be the aim of the next section.

2.2. Analysis based on the site-dependent mean-field (SDMF) solutions

According to the SDMF approach, the mean-field is (thermally) averaged at each site individually, thus introducing a spatial dependence in the solution. The resulting Hamiltonian reads

$$\mathcal{H} \approx -J \sum_i \left(\sum_{j=n.n.} < \sigma_j > + h_i + h \right) \sigma_i \tag{23}$$

which yields for the magnetisation at the ith site

$$m_i = 2\theta \left(\sum_{j=n.n.} m_j(h) + h_i + h \right) - 1 \tag{24}$$

where $\theta(\cdot)$ stands for the Heaviside step function and

$$m_i =< \sigma_i > \tag{25}$$

similarly to (5). It is recalled that the summation is carried out considering only the nearest neighbours (n.n.) of each spin. Notice that (24) is the zero-temperature limit of the SDMF solution. Averaging over the random field values, we obtain the relation

$$m_i(h) = 1 - 2 \int_{-\infty}^{-\sum_j m_j(h) - h} \rho(h_i)\, dh_i. \tag{26}$$

which is the generalisation of (10).

Due to the much more complicated mathematical structure of (26), where m_i is coupled with all neighbouring spins, we have to proceed to the analysis numerically. Hence, in order to obtain the m_i distribution, the system lattice is first truncated along its $z/2$ spatial dimensions (3 in this case). Let N be the total number of the considered (finite) lattice sites. The random field h_i is then evaluated at the lattice sites using a random number generator following the (8) distribution with the disorder r as tuning parameter. Fixing the lower and upper limits of the external field, i.e. setting $h \in [-h_{max}, h_{max}]$, we proceed to a uniform discretisation of the magnetic field, namely

$$h^{(k)} = -h_{max} + k\Delta h,\ k = 0, \ldots, N_h \tag{27}$$

with $\Delta h = 2h_{max}/N_h$. Varying the field $h^{(k)}$, the system of N coupled equations (24) is solved iteratively using a fixed-point scheme until the relative error drops under a predefined precision threshold ϵ, that is

$$\frac{\sum_i \left(\left[m_i^{(k)} \right]_{n+1} - \left[m_i^{(k)} \right]_n \right)^2}{\sum_i \left(\left[m_i^{(k)} \right]_n \right)^2} \leq \epsilon \tag{28}$$

n being the iteration number of the fixed-point algorithm.

Special care needs to be taken in order to properly account for the hysteresis. Once the system (24) has converged for the kth step of the field discretisation, the obtained solution $m_i^{(k)}$ is set as initial value for the solution of the $(k+1)$th step. This is important since, if we provide the algorithm with the same initial value at each step

(say for example 0 everywhere), the convergence will be biased to a subspace of the original configuration space, thus avoiding the local minima lying at the vicinity of the system state at the kth step. It is in fact these minima which stand for the metastable states responsible for the hysteresis. As far as the initial value for $k = 0$ is concerned, we set $m_i^{(0)} = -1$, assuming that the system has been prepared to the (negative) saturation.

In order to describe a complete cycle, the field is first increased to its maximum value, according to (27), and then reduced back to $-h_{max}$ by flipping the $h^{(k)}$ sequence. The magnetisation curves obtained by the above described approach for a number of different disorder values are illustrated in Fig. 3a. The magnetisation value depicted is the mean value throughout the lattice, that is

$$m^{(k)} = \frac{1}{N}\sum_{i=1}^{N} m_i^{(k)}. \tag{29}$$

All these solutions demonstrate hysteresis, which is different from the situation we observed with the scalar mean-field theory (cf. Fig. 1a). The explanation should be sought to the nature of the configuration space landscape that the SDMF algorithm explores during the minimisation of (28) and the passage from the possible metastable states, as discussed above. A thorough discussion about the behaviour of SDMF for RFIM solutions out of equilibrium can be found in [13]. Interestingly, these results could have hardly been obtained by Monte-Carlo simulations, which by construction tend to reach the equilibrium state [6].

The second order transition discussed in the previous paragraph is also observed with the SDMF solution, yet the value of the critical disorder is different. In fact, the SDMF estimate of the critical value is $r_c \approx 3.2$ in comparison with the higher value of $r_c \approx 5.0$ obtained via the mean-field theory. The evolution of the magnetisation jump Δm as a function of the normalised distance from the critical disorder $1 - r/r_c$ is shown in Fig. 3b. Since the SDMF solution fluctuates between successive simulations, a number of independent simulations is carried out and the results are averaged to the curve of Fig. 3b. In order to further test this result, we examine if it exhibits a power-law behaviour in the vicinity of the critical point for $r < r_c$. A first order curve is fitted to the simulation points in a log-log representation

$$\log(\Delta M) = \beta \log(1 - r/r_c) + c \tag{30}$$

and the coefficient β is determined. The resulting curve is compared in Fig. 3b with the average curve thus confirming the power-law behaviour with a critical exponent $\beta = 0.662$, close to the $1/2$ value obtained by the classical mean-field theory [9].

The magnetic susceptibility along the ascending hysteresis branch obtained by the SDMF solution for three distinct disorder values are depicted in Fig. 4. The susceptibility plots have been obtained by numerical differentiation of the corresponding magnetisation curve, namely

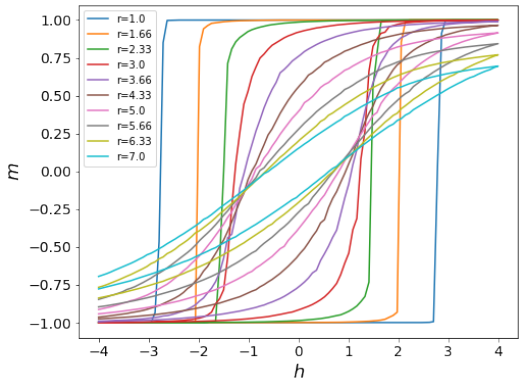

(a)

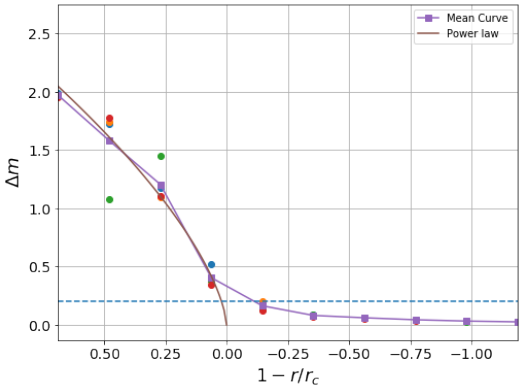

(b)

Figure 3: (a) SDMF solution for the magnetisation curve for different disorder values. (b) Magnetisation jump at h_c as a function of the distance from the critical disorder $1-r/r_c$. The critical disorder value can be estimated as $r_c \approx 3.2$. The numerical curve is the average of four successive simulations (pointed by the different coloured dots). The supercritical behaviour can be described by a power law of the type $(1 - r/r_c)^{\beta}$.

$$\chi^{(k)} \approx \frac{m^{(k)} - m^{(k-1)}}{\Delta h}. \tag{31}$$

The variation of the susceptibility is not smooth as it becomes clear from Fig. 4. This effect is a manifestation of the discontinuous change of the magnetisation value along the hysteresis, in a way that it strongly resembles the Barkhausen jumps. Note that this "noise" reaches its maximum around the coercive field value, which is in accordance with the experiment.

In Fig. 4, the numerical curves are fitted to a Lorentzian and a Gaussian distribution. In a resemblance with the previous results for the mean-field theory, the Lorentzian distribution fits quite nicely with the numerical results for almost the entire window of the field values. The Gaussian distribution gives also satisfactory results for higher disorder values, it deviates slightly with $h < h_c$ for $r = 3.6$, i.e. just after the phase transition. It should be also noticed the better fit of the Gaussian distribution for $h > h_c$.

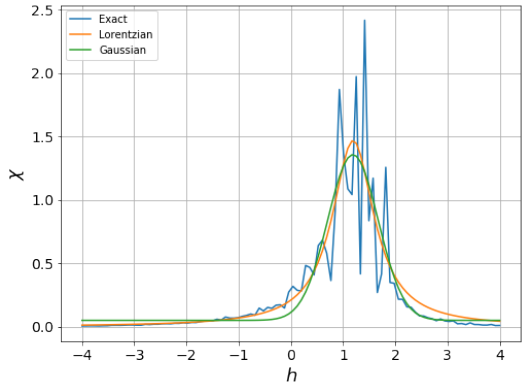

(a)

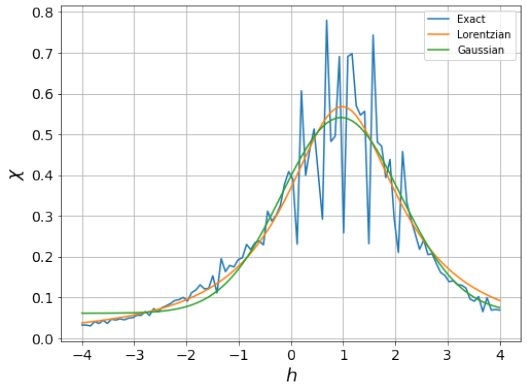

(b)

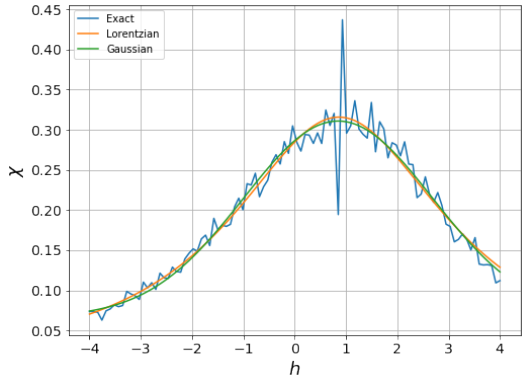

(c)

Figure 4: Fitted Lorentzian and Gaussian distributions to the susceptibility SDMF solution across the coercive field (ascending branch) for three different disorder values: (a) $r = 3.6$, (b) $r = 5.0$ and (c) $r = 6.33$.

The reciprocal susceptibility values at the coercive field χ_c obtained by the fitted Lorentzian (cf. (18)) versus the disorder r are plotted in Fig. 5. The plot implies a linear correlation between the two values, which is confirmed by the least-square fit of a first order polynomial. This is in straight analogy with (19), obtained analytically for the mean-field theory. It is also interesting to compare the numerical value of the linear term coefficient, determined by the least-square fit as ~ 0.97 with the $\sqrt{\pi/2} = 1.25$ of the analytical expression.

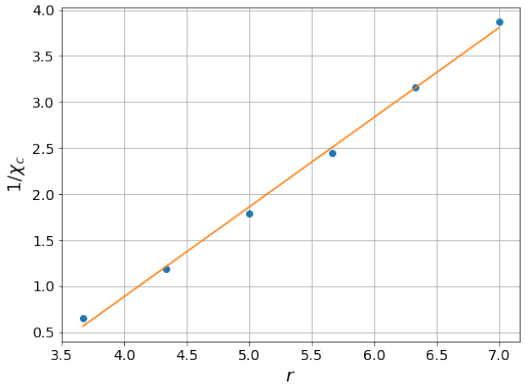

Figure 5: Susceptibility values obtained by the fitted Lorentzian distribution at the coercive field as function of the disorder.

3. Application to soft steels

The above results have been confronted with the experimental curves obtained for two soft steel grades. The considered specimens stem from cold-rolled laminated sheets subjected thereupon to isothermal annealing at different temperatures and for different holding times [1–3].

Two set of samples were considered for this study. One set from industrially produced $Ti - Nb$ stabilized interstitial free (IF) ultra low carbon (ULC) steel, with composition 0.003%C-0.11%Mn-0.02%Nb-0.012%Ti, cold rolled to a final thickness of 0.8 mm through a reduction of 75% [14] and a second set from extra low carbon steel (ELC), with composition 0.03%C-0.19%Mn-0.13%Al-0.0035%N - 0.012%P-0.01% Si, that had been industrially produced and cold rolled to a final thickness of 0.3 mm through a reduction of 84% [1, 2, 15]. The samples had been thermal treated in laboratory. First heated in an argon atmosphere, at a rate of 20°C/s to reach a temperature within the range of 300-550°C, followed by holding times at these temperatures in the range of 1 s to 10,000 s ($\approx$ 2.8 h). The annealing treatments were then interrupted and the samples quenched in helium to reach room temperature at a rate close to -60°C/s.

The annealing time and temperatures were selected so that the thereupon induced microstuctural changes to be dominated by the recovery procedure without triggering recrystallisation. In this way, the major impact of the annealing procedure is restricted to the decrease and rearrangement of the dislocation density with the grain size remaining intact.

Near saturation major magnetic B-H hysteresis loop measurements were made at 1 Hz using a single sheet tester system available at author's laboratory [16], with an encircling coil wound around the samples with maximum magnetic field strengths applied of about 4100 A/m. The effect of the annealing treatment on the experimental BH hysteresis loops can be found for cold rolled IF steel annealed at 350°C and 550°C and at 450°C at [14] and at [15] for the cold rolled ELC steel annealed at 300°C and 450°C.

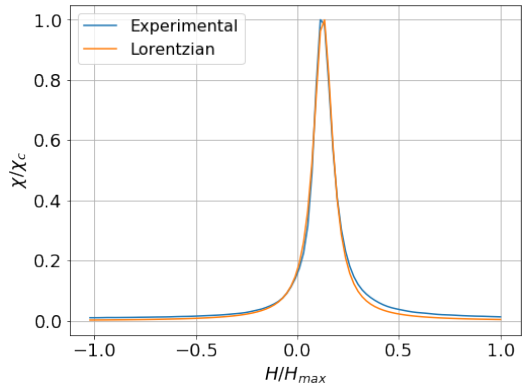

(a)

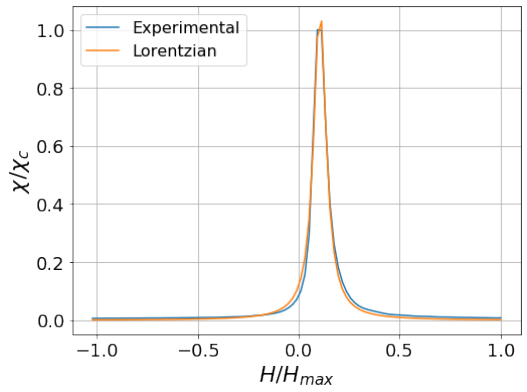

(b)

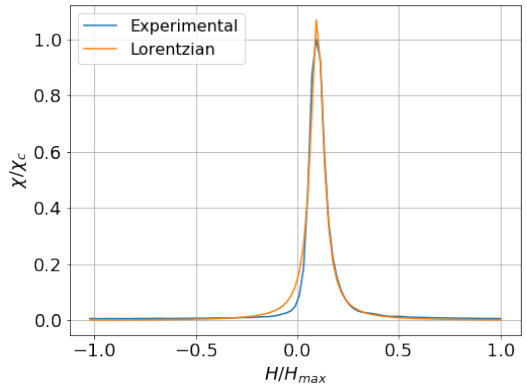

(c)

Figure 6: Fitted Lorentzian to the experimental IF susceptibility curves for three different annealing conditions: (a) Cold-rolled (no treatment), (b) 1000 s at 350°C (623 K) and (c) 1000 s at 550°C (823 K).

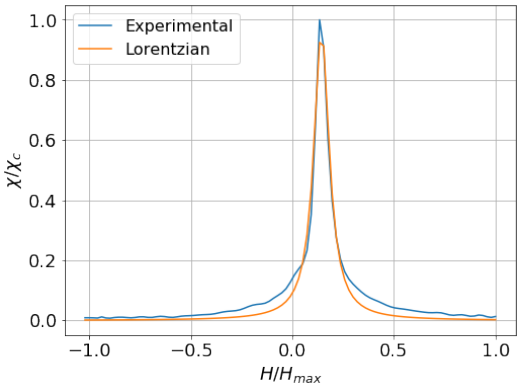

(a)

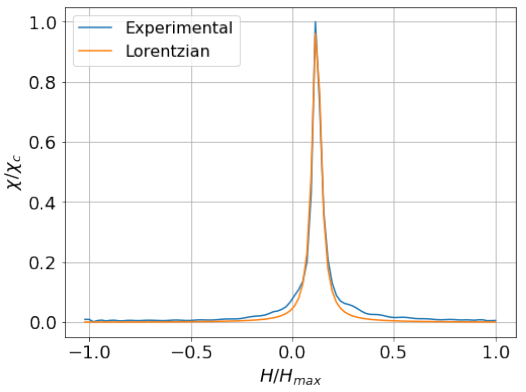

(b)

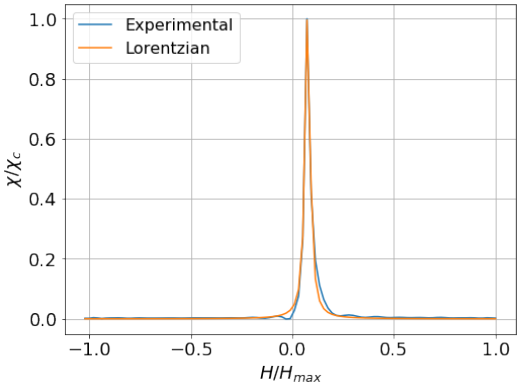

(c)

Figure 7: Fitted Lorentzian to the experimental ELC susceptibility curves for three different annealing conditions: (a) 51 s at 300°C (573 K), (b) 51 s at 400°C (673 K) and (c) 36 min at 500°C (773 K).

Assuming that the changes to the specimen microstructure can be captured by a random field with different values of disorder r, and applying the above discussed approach, the measured susceptibility curves are fitted to the Lorentzian approximation described in (22). The results for the two grades and for three different annealing conditions are shown in Fig. 6 and Fig. 7, respectively. The susceptibility curves are plotted as functions of the measured magnetic field H and not the normalised h.

It is interesting to trace the evolution of the fitted maximum value of susceptibility χ_c as a function of the annealing time. According to the previous analysis, the inverse maximum susceptibility is proportional to the system disorder r. Hence, one could expect that χ_c^{-1} may provide some qualitative image of the recovery process. The corresponding plots of the inverse susceptibility evolution with time for the different annealing temperatures and the two considered steel grades are given in Fig. 8. The nearly monotonous decrease of the inverse susceptibility with the annealing time (with the exception of the short times at

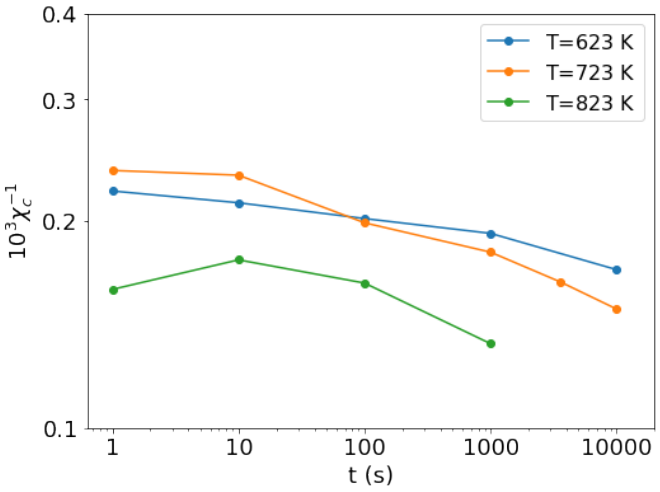

(a)

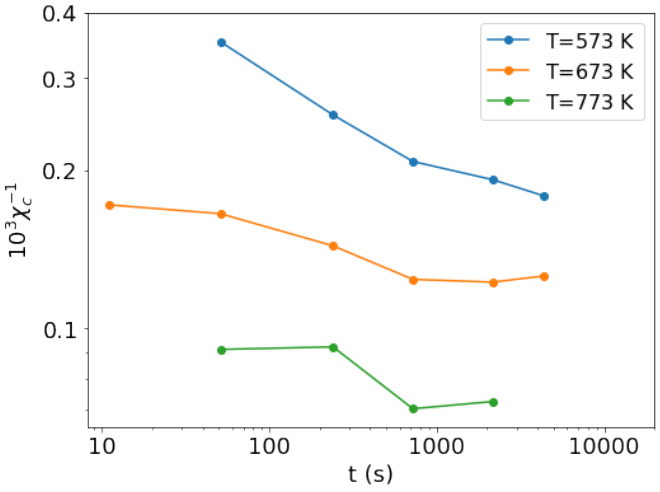

(b)

Figure 8: Evolution of the inverse susceptibility with annealing time at different annealing temperatures: (a) IF steel, (b) ELC steel.

high annealing temperature for the IF) seems to be in accordance with the fact that the dislocation density is decreasing during the recovery.

A similar statement can also be made concerning the annealing temperature. In fact, the relative position of the curves, except for some points at low annealing times of the IF steel, follows the decrease in the dislocation density with increasing temperature.

A question that might be arisen concerns the validity of the zero-temperature approach for the studied case. It should be recalled that the Curie point, indicating the temperature region where thermal fluctuations become important, lies around 770°C (1043 K) for carbon steels. All the magnetic measurements were made at room temperature once the samples had been removed from the annealing simulation device, which means that we are located at 29% of the Curie temperature (ratio calculated after conversion to Kelvin), and we recall by the corresponding phase diagrams that the magnetisation curve descends very steeply just before the Curie point to reach zero [17]. Precise measurements at high temperatures for similar steel grades have been communicated in the recent literature which supports this argument [18, 19]. We can hence conclude that the random field effect is dominant against thermal fluctuations for these temperatures. Moreover, outside the critical range of the transition (usually a few degrees from the critical temperature at most) the system is expected to be described from the mean-field approach. In our case this condition is fulfilled ($T_{max} \sim 0.29T_c$).

One might come to the same conclusion by considering comparisons of the critical exponents relative to Barkhausen avalanche characteristics with the corresponding experimental values [11, 20]. The experimental results for these studies have been obtained in room temperature conditions as well.

Conclusions

A very simple random field spin model has been used for the interpretation of the behaviour of the differential susceptibility curves around the coercive field. It appears that the implicit solution of the RFIM for small field values can be adequately approximated by a Lorentzian function, whose peak (corresponding susceptibility at the coercive field) provides a measure for the system disorder. This approximation explains the nearly Lorentzian profile of the experimental susceptibility curves, and is theoretically supported by the scaling laws at the coercive field for supercritical disorder values.

Although the highly simplified conceptual image of the disorder used by the model should not be directly related with the real material randomness translated to a dislocation distribution (in the considered case of steels subjected to recovery), this model "randomness" could still serve as a figure-of-merit for the real randomness, as Fig. 8 implies.

Caution should be also taken concerning the model domain of validity. One must not forget that the Ising model considers spins oriented in one direction, hence it is restricted (at least theoretically) to materials with strong anisotropy, where the spins tend to align with the easy magnetisation axis. A more thorough study should take this limitation into account, and one must be aware that the above analysis may not hold for different families of materials. In such cases the use of more sophisticated models, like the XY or the Heisenberg model may be indispensable.

Acknowledgements

A. Martínez-de-Guerenu and D. J. Badiola acknowledge funding from the Basque Government under the Elkartek Program, Project Nos. KK-2019/0010 and KK2021/00082.

References

[1] A. Martínez-de-Guerenu, F. Arizti, M. Díaz-Fuentes, I. Gutiérrez, Recovery during annealing in a cold rolled low carbon steel. Part I: Kinetics and microstructural characterization, Acta Mater. 52 (12) (2004) 3657–3664. doi:10.1016/j.actamat.2004.04.019.

[2] A. Martínez-de-Guerenu, F. Arizti, I. Gutiérrez, Recovery during annealing in a cold rolled low carbon steel. Part II: Modelling the kinetics, Acta Mater. 52 (12) (2004) 3665–3670. doi:10.1016/j.actamat.2004.04.020.

[3] A. Martínez-de-Guerenu, K. Gurruchaga, F. Arizti, Nondestructive characterization of recovery and recrystallization in cold rolled low carbon steel by magnetic hysteresis loops, J. Mag. Mag. Mater. 316 (2) (2007) e842–e845. doi:10.1016/j.jmmm.2007.03.110.

[4] T. Nattermann, Theory of the random field Ising model, in: A. P. Young (Ed.), Spin Glasses and Random Fields, Vol. 31, World Scientific, 1997, pp. 277–298. doi:10.1142/9789812819437_0009.

[5] D. P. Belanger, A. P. Young, The random field Ising model, J. Mag. Mag. Mater. 100 (1991) 272–291. doi:10.1016/0304-8853(91)90825-U.

[6] M. E. J. Newman, G. T. Barkema, Monte Carlo study of the random-field Ising model, Phys. Rev. E 53 (1996) 393–404. doi:10.1103/PhysRevE.53.393.

[7] J. P. Sethna, K. A. Dahmen, O. Perković, Random-field Ising models of hysteresis, in: G. Bertotti, I. D. Mayergoyz (Eds.), The Science of Hysteresis, 1st Edition, Vol. II, Academic Press, 2006, Ch. 2, pp. 105–179.

[8] J. P. Sethna, K. A. Dahmen, S. Kartha, J. A. Krumhansl, B. Roberts, J. Shore, Hysteresis and hierarchies: Dynamics of disorder-driven first-order phase transformations, Phys. Rev. Lett. 70 (21) (1993) 3347–3350. doi:10.1103/PhysRevLett.70.3347.

[9] K. A. Dahmen, J. P. Sethna, Hysteresis avalanches, and disorder-induced critical scaling: A renormalization-group approach, Phys. Rev. B 53 (22) (1996) 14872–14905. doi:10.1103/PhysRevB.53.14872.

[10] M. C. Kuntz, J. P. Sethna, Noise in disorder systems: The power spectrum and dynamic exponents in avalanche models, Phys. Rev. B 62 (17) (2000) 11699–11708. doi:10.1103/PhysRevB.62.11699.

[11] O. Perković, K. A. Dahmen, J. P. Sethna, Avalanches, Barkhausen noise, and plain old criticality, Phys. Rev. Lett. 75 (24) (1995) 4528–4531. doi:10.1103/PhysRevLett.75.4528.

[12] K. A. Dahmen, J. P. Sethna, M. C. Kuntz, O. Perković, Hysteresis and avalanches: phase transitions and critical phenomena in driven disordered systems, J. Mag. Mag. Mater. 226-230 (Part 2) (2001) 1287–1292. doi:10.1016/S0304-8853(00)00749-6.

[13] G. S. Grest, C. M. Soukoulis, K. Levin, Comparative Monte Carlo and mean-field studies of random-field Ising systems, Phys. Rev. B 33 (11) (1986) 7659–7674. doi:10.1103/PhysRevB.33.7659.
URL https://link.aps.org/doi/10.1103/PhysRevB.33.7659

[14] A. Martínez-de Guereñu, M. Oyarzabal, F. Arizti, I. Gutiérrez, Application of coercive field measurements to the evaluation of recovery and recrystallization in cold rolled interstitial free (IF) steel, in: Microalloying for New Steel Processes and Applications, Vol. 500–501 of Materials Science Forum, 2005, pp. 647–654. doi:10.4028/www.scientific.net/MSF.500-501.647.

[15] A. Martínez-de-Guerenu, K. Gurruchaga, F. Arizti, Use of magnetic techniques for characterisation of the microstructure evolution during the annealing of low carbon steels, in: Proc. 9th European Conference on Non-Destructive Testing (ECNDT), 2006, pp. 1–11.

[16] M. Soto, A. Martínez-de-Guerenu, K. Gurruchaga, F. Arizti, A completely configurable digital system for simultaneous measurements of hysteresis loops and Barkhausen noise, IEEE Trans. Instrum. Meas. 58 (5) (2009) 1746–1755. doi:10.1109/TIM.2009.2014510.

[17] R. M. Bozorth, Ferromagnetism, Wiley-IEEE Press, New York, 1993.

[18] A. Boehm, I. Hahn, Measurement of magnetic properties of steel at high temperatures, in: IECON 2014 - 40th Annual Conference of the IEEE Industrial Electronics Society, 2014, pp. 715–721. doi:10.1109/IECON.2014.7048579.

[19] J. W. Wilson, L. Zhou, C. L. Davis, A. J. Peyton, High temperature magnetic characterisation of structural steels using Epstein frame, Meas. Sci. Technol. 32 (12) (2021) 125601. doi:10.1088/1361-6501/ac17fa.

[20] G. Durin, S. Zapperi, The Barkhausen effect, in: G. Bertotti, I. D. Mayergoyz (Eds.), The Science of Hysteresis, 1st Edition, Vol. II, Academic Press, 2006, Ch. 3, pp. 181–267.